Fire Technology, 50, 565–587, 2014

DOI: 10.1007/s10694-013-0323-z

Experimental and Numerical Study of the Interaction Between Water Mist and Fire in an Intermediate Test Tunnel

E. Blanchard, P. Fromy and P. Carlotti, CSTB—Centre Scientifique et Technique du Bâtiment, 84 avenue Jean Jaurès, Champs sur Marne, 77447 Marne-La-Vallée Cedex 2, France*

P. Boulet, LEMTA—Laboratoire d'Énergétique et de Mécanique Théorique et Appliquée Nancy Université, CNRS, Faculté des Sciences et Technologies, BP 70239, 54506 Vandoeuvre Cedex, France

S. Desanghere, Sonovision division Ligeron, 3 cours Albert Thomas, 69003 Lyon, France

J. P. Vantelon and J. P. Garo, Institut P', UPR CNRS 3346—Département Fluides, Thermique, Combustion—ENSMA, BP 40109, 86961 Futuroscope Chasseneuil, France

Received: 16 March 2012/**Accepted:** 4 January 2013

Abstract. The paper deals with interaction between water mist and hot gases in a longitudinally ventilated tunnel. The work aims at understanding the interaction of mist, smoke and ventilation.The study is based on one intermediate tunnel test and an extensive use of the computational code Fire Dynamics Simulator (FDS, NIST). The approach consists first of reconstructing the test with the CFD code by defining the relevant numerical parameters to accurately model the involved water mist system. Then, it consists of handling from the local data the complicated flows generated by the water mist flooding on the one hand and by fire and ventilation on the other hand. The last stage consists in quantifying each mechanism involved in interaction between water mist and hot gases. There are three main results in this study. Firstly, the CFD code prediction is also evaluated in this configuration, with and without water mist. Before the mist system activation, the agreement is satisfactory for gas temperatures and heat flux. After the activation time, the CFD code predicts well the thermal environment and in particular its stratification. Secondly, water mist plays a strong thermal role since in the test studied, roughly half of the heat released by fire is absorbed by water droplets. Thirdly, heat transfer from gaseous phase to droplets is the main mechanism involved (73%). The remaining heat absorbed by droplets results from tunnel surface cooling which represents (9%) and radiative attenuation (18%).

Keywords: Water mist, Fire, Tunnel, Interaction phenomena, CFD, Model test

* Correspondence should be addressed to: E. Blanchard, E-mail: Elizabeth.mf.Blanchard@gmail.com

Nomenclature

C_p	Heat capacity (J kg^{-1} K)
h	Heat transfer coefficient (W m^{-2} K^{-1})
L_v	Latent heat of vaporization (J kg^{-1})
m	Mass (kg)
Q	Energy (W)
S	Surface area (m^2)
T	Temperature (K)
t	Time (s)
V	Volume (m^3)
V_c	Control volume (m^3)

Greek symbols

ρ	Density (kg m^{-3})

Subscripts

g	Gas property
fire	Fire property
p	Water droplet property
d	Tunnel openings property
w	Tunnel walls property

List of abbreviations

HRR	Heat release rate

1. Introduction

In tunnel fire safety, fires that have occurred for one decade have played a major role since they have highlighted the potential importance of human and financial consequences. Therefore, requirements for road tunnels have significantly evolved. For instance, France can be cited with the Inter-Ministry circular of August 2000 (replaced in March 2006 by circular 2006-20) for national road tunnels and the European circular of April 2004 for the trans-European road tunnel network. These requirements have reinforced the strategy in case of fire which aims at maintaining a free-smoke area near the roadway as long as possible. This strategy has two main objectives. At first, it promotes the self-evacuation of people. Then, it aims at improving the operating conditions of fire-fighters. This fire safety management is ensured by a large sample of systems, including ventilation systems.

In monitoring technological development, authorities and tunnel owners are still looking for new ways/systems for ensuring a higher safety level. In this context, Water-based Fixed Fire Fighting Systems (WFFFS) are more and more considered as a way to improve fire safety in tunnels via controlling (and even sometimes suppressing) fire spread and heat release. In 2008, the world road association PIARC even expressed the opinion that a fire-fighting system *is one of many system types available to deliver user safety and infrastructure protection* [1]. Among these WFFFS, we focus here on ''water mist'' systems producing the

smallest droplets and involving the lowest sprayed water quantity [2]. The use of water mist has grown at a very high rate since the seventies, starting with the need to find an alternative to the banned halogen-based fire suppressing agents. There are two main differences between water mist systems and conventional sprinkler systems which result from breaking water into a cloud of very small droplets. Firstly, this spraying increases greatly the surface area available for exchanging heat with surrounding gases. Secondly, it strongly influences droplet momentum. The time period during which droplets are in suspension in the gaseous phase can consequently be significantly longer.

1.1. Phenomena Involved in Interaction Between Water Mist and Hot Gases

When water is sprayed in the vicinity of a fire characterized by hot gases and important thermal radiation, four major mechanisms are identified [3]. Firstly, an amount of heat is transferred from gases and surfaces to water droplets. Droplets are also heated and evaporated by this "heat sink" while gases and surfaces are cooled down. Secondly, the phase change from liquid to vapor induces a high volumetric expansion rate. This phenomenon prevents the mixing between fresh air and combustible vapor, acting like an inert gas, thus being able to reduce the intensity of combustion reactions. Thirdly, water droplets interact with thermal radiation emitted by flames, surrounding solid surfaces and hot gases by absorption and scattering effects [4, 5]. Thus, this phenomenon can limit the fire propagation (to other vehicles trapped in the tunnel for instance) and even affect the fuel burning rate by attenuating heat feedback to fuel [6, 7]. Fourthly, water spray may interact with smoke layer due to gas cooling and momentum exchange. This interaction may induce a thermal destratification of the environment.

The importance of these four phenomena depends on the fire environment (fire heat release, ventilation, etc.) and the water mist characteristics (droplet size, spray pattern, etc.). For instance, very small droplets are rapidly decelerated after leaving the nozzle. Also, their residence time in the air is longer thus promoting radiative attenuation and gas cooling but their ability to penetrate the flame zone is reduced [8], making it difficult to steer them toward a given target. The scientific literature reports a large number of research campaigns, conducted from the laboratory scale up to real scale such as compartment and tunnel. Among them, one may cite those focused on one fundamental phenomenon (for instance [9, 10]), on water mist effect on HRR [11] or even, those studying the problem more globally (for instance [12, 13]).

1.2. Research on Water Mist in Tunnel Configuration

To date, a few large-scale tests have been conducted in tunnels using a water mist system like the European campaign UPgrading of existing TUNnels [14] or the German campaign Safety Of Life In Tunnels [13]. Such real scale tests are very expensive because a large number of sensors are required to track smoke and hot gases. That is generally done with thermocouple trees installed at several distances from the fire location. Large-scale tests are very useful to test water mist in real conditions, by involving real fire load and fluid flow. However, it could be

difficult, and even impossible, to draw general conclusions concerning the influence and the efficiency of such a system [15].

Even if there are still some difficulties in properly scaling the thermal radiation attenuation by the sprays and the water droplet size (except by using geometrically similar spray nozzles) [16], reduced scale tests could present a great interest, for instance to accurately study one phenomenon in particular, to carry out a parametric study or to provide useful correlations. In fact, they are relatively inexpensive and easy to conduct and they allow better repeatability [17]. For instance, Ingason in [18] studied the influence of several parameters such as the water flow density, the number of nozzles and the longitudinal ventilation rate on the thermal environment and fire spread in a model tunnel (1/23). Following the same idea, Chen et al. [19] studied in a model tunnel (1/10) the influence of longitudinal velocity and the interval between mist nozzle and fire source on water mist fire suppression.

The measurements made on model or real scale experiments can be used as a basis for numerical research. Computational model can be proposed and experimental base are useful to validate numerical codes for specific scenarios. Moreover, after a preliminary validation, CFD models allow us to simulate many other situations for which there is no experimental data available by giving at least orders of magnitude. However, to date, only a few papers involving numerical modeling of mitigation systems in tunnels have been published [20–22]. Among them, Trelles and Mawhinney [22] simulated with the Fire Dynamics Simulator code (FDS code) (version 4) one of the largest fire tests conducted by Marioff Corporation Oy. involving a high pressure water mist system. By setting the HRR curve, they obtained a reasonable degree of agreement of computational results with the conditions measured in the tests. More precisely, whereas the backlayering disappearance was well predicted, the gaseous phase temperature downstream of the fire location was overestimated by the computational code. The authors explained this difference with the moist environment in the test that affects the temperature measurement.

1.3. Purpose of the Present Study

The present paper deals with the interaction phenomena between water mist and hot gases in a longitudinally ventilated tunnel. The work aims at understanding the interactions between water mist, tunnel longitudinal ventilation and hot smoke flow in one tunnel test. To do this, it makes an extensive use of the Fire Dynamics Simulator code (FDS developed by NIST in cooperation with VTT [23, 24]). The approach consists first of reconstructing the test. Secondly, it consists of handling from the local data the complicated flows generated by water mist flooding on the one hand and by fire and ventilation on the other hand. The last stage consists of quantifying each mechanism involved in interaction between water mist and hot gases.

The test studied belongs to a campaign carried out in an intermediate tunnel, the scale ratio with a real tunnel being in the order of one third. The use of such a reduced scale aims at studying fire phenomena in a more affordable way than

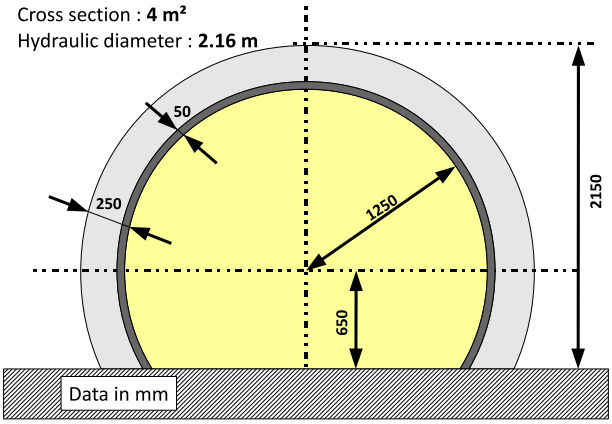

Figure 1. Cross-sectional view of the tunnel.

with real scale experiments and in a more realistic way than with a laboratory scale. In this campaign, 28 tests were conducted involving three types of fire fuel, the two longitudinal ventilation regimes (sub-critical and supercritical), and three water mist system configurations. Among them, the test studied is selected because it involves a low water flow rate. Consequently, mist activation does not induce strong fire suppression and associated important gas cooling. It allows us to assess the CFD code when the mist system is activated, as well as to study the fire environment during this time period. Since the scope of the present study concerns the thermal environment, fire suppression is beyond it. The fire suppression model is thus deactivated and not studied here. For your information, during the test campaign in the intermediate tunnel, one test was performed in similar conditions but with a higher number of nozzles (14 nozzles). Fire was suppressed in less than 1 min which is efficient but which does not allow us to study gas cooling properly [25].

2. Intermediate Tunnel Test

2.1. Tunnel Description, Longitudinal Ventilation and Instrumentation

The model tunnel is horizontal and completely belowground. It is 43 m long with a semi-circular cross section around 4 m^2 and a 2 m hydraulic diameter (see Figure 1 for the cross-sectional view of the tunnel). Walls are covered by fire resistant mortar cement with well-know thermal characteristics. Floor is made of concrete.

A fan is mounted at the downstream side of the tunnel. It allows us to control the longitudinal air flow, by extracting a roughly constant gas volume flux. A longitudinal velocity of around 3.0 m/s is set, corresponding to a supercritical ventilation regime when all the smoke produced by the fire is extracted from one end of the tunnel [26].

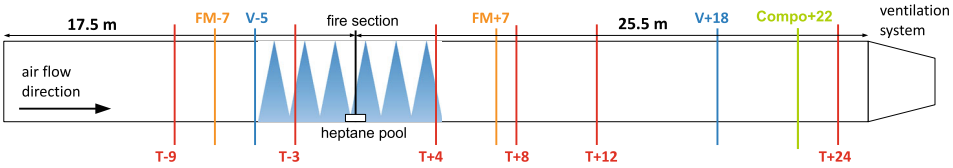

Figure 2. Position of measurement sections (*T* gas temperature, *V* gas velocity, *FM* heat flux and Compo:gas composition). Nozzle locations are represented by sprays. *Numbers* are distances in m.

In addition to fuel mass, four quantities are measured: gas temperature, gas velocity, heat flux and gas composition. Sensors are located on four sections upstream and seven downstream of the fire location (see Figure 2). Instrumentation is deeply detailed in Ref. [26] with related characteristics and uncertainties.

2.2. *Water Mist System*

The water mist system installed by a manufacturer is composed of six nozzles installed on the same row, located on the center line of the tunnel. The nozzles are located between 4 m upstream and 3.5 m downstream of the fire location, 1.5 m apart (see Figure 2). All the nozzles are manually activated at the same time, 300 s after ignition. With an operating pressure around 90 bars, the water flow rate injected at each nozzle is close to 5.5 l/min, corresponding to a total mist discharge rate of around 33 l/min. This mist discharge is rather low compared with the other tests of the campaign (77.0 l/min) or with standard application (higher than 689 l/min in Ref. [22]).

Each water mist nozzle in the intermediate tunnel has four lateral and one central orifices (see Figure 3). Each spray pattern is conic and ejection angle is evaluated at 20° by Phase Doppler Analysis [27] (PDA, a description of this technique is given in Ref. [8]). Each orifice diameter is around 0.5 mm. As to the injected water flow rate, the initial droplet velocity could be estimated at around 60 m/s. This value is a rough estimate since such small droplets strongly decelerate, even along a short distance.

2.3. *Fire Load*

The test is conducted with a fire load produced by a 0.5 m^2 heptane pool (1.0 m long, 0.5 m wide and 0.1 m deep). The test duration corresponds to the heptane complete burning. This liquid fuel is chosen in order to ensure repeatability between experiments, and to reduce uncertainties related to estimation of heat release rate (HRR). HRR is deduced from fuel weight loss monitoring based on oxygen consumption monitoring [28]. As shown on Figure 4, HRR deduced using the two methods is almost the same before mist activation. After that, deduced HRR is clearly different. This is attributed to the water droplets sprayed at the fire location that may alter the heptane pool weight monitoring.

As mentioned previously, the sprayed water flow rate is low. The main consequence is that HRR reaches a higher value during the mist period (300 s to 600 s)

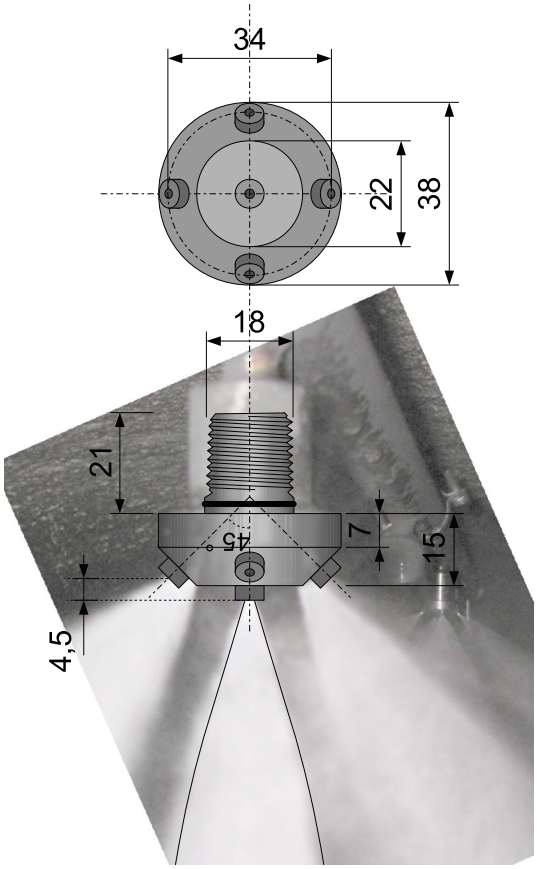

Figure 3. Nozzle geometrical characteristics.

than at the activation time 300 s. HRR evolution is attributed to multiple concomitant phenomena. HRR first drops due to potential oxygen depletion and a first cooling stage for fire load and gas enhanced to the fire. Then it further increases, potentially due to various effects: turbulence enhancement influencing combustion processes, or a typical effect already observed in pool fires when the fuel volume tends to zero, which involves a sharp peak because all the substrate reaches the boiling point.

3. Tunnel Test Simulation

3.1. Numerical Model Description

The present work makes use of the Fire Dynamics Simulator (FDS, developed by NIST, USA [23, 24]), which is a 3D CFD model designed to simulate low-speed, thermally-driven flows. This numerical tool is widely employed in the fire commu-

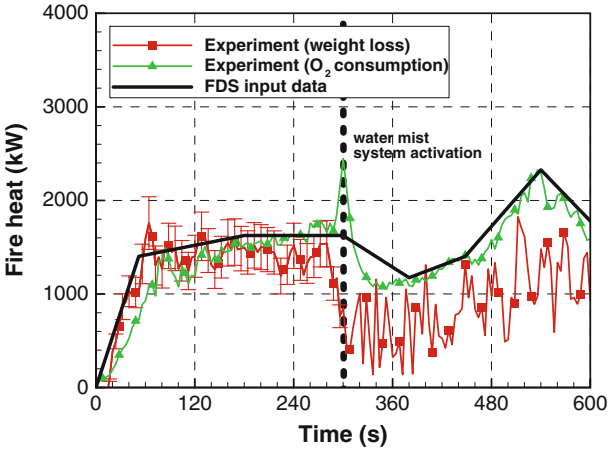

Figure 4. HRR deduced from fuel weight loss and oxygen consumption. The smoothing function used as input in the simulation is also presented.

nity, generally in order to evaluate fire consequences in buildings. FDS has also been used to simulate tunnel fires, especially by McGrattan and Hamins [29], Cochard [30] and Trelles and Mawhinney [22]. The ability of the version used here (version 5.4) to reconstruct the fire environment without the application of water mist has been presented in details in [26], on the basis of one test performed within the one third test gallery used here. The paper [26] shows that agreement between FDS predictions and temperature measurements is satisfactory at different distances from the fire. Air flows are also well reproduced in the simulations, the measurement difference staying within the overlapping uncertainty limits.

Concerning spray modeling, FDS uses an Eulerian-Lagrangian approach to simulate the turbulent transport of evaporating droplets. This means that trajectories of water droplets are individually tracked. In order to reduce the computational cost, only a limited number of droplets are tracked. Each droplet in the calculation is assumed to represent many others of similar size and trajectory. The droplets tracked have to constitute a representative sample of the entire spray. The spray characteristics are defined at the injection point by a considerable number of parameters such as fluid thermal properties, droplet size distribution and injection features (spray pattern, volumetric flow rate, etc.). In particular, the droplet size distribution is represented by a probability function that describes the fraction of the water volume transported by droplets whose dimension is less than a given diameter. In FDS, the default probability function is a combination of log-normal and Rosin–Rammler distribution. Droplet trajectories are calculated by solving the momentum conservation. Heat transfer between the droplets and the surrounding gas is computed using correlations preserving the equilibrium with the gaseous phase inside each grid cell. When a particle strikes an obstacle, it sticks (a new speed and a new direction) until it is evaporated.

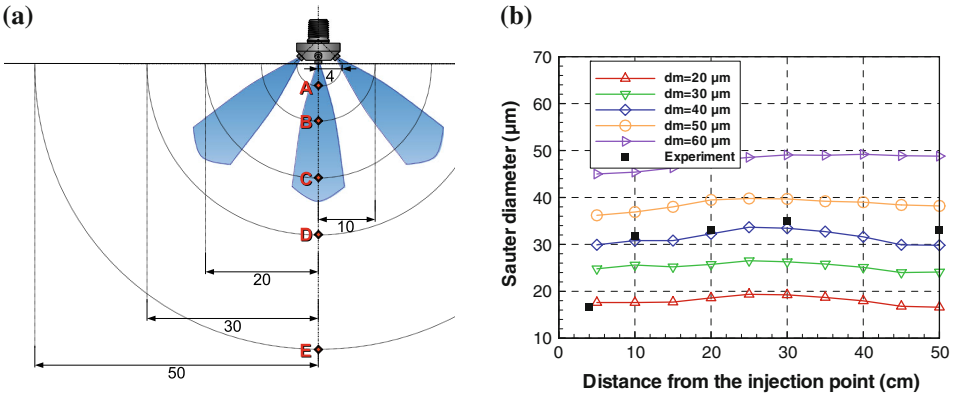

Location of droplet size measurement in PDA

Predicted and measured droplets size along the central vertical axis

Figure 5. Droplet size characterization.

3.2. Input Data Definition

Simulations are carried out with the FDS code (version 5.4). The computational domain includes the tunnel, the ventilation system at the downstream side (by setting an exhaust volume flow), and a free area at the upstream side. The last area is simulated in order to better promote the flow turbulence in the tunnel. Concerning the spatial and angular discretizations, cubic grid cells with a 10 cm side are used (which corresponds to 440,000 cells, a number resulting from a sensitivity analysis) and the unit sphere is divided into 512 solid angles for the radiative transfer model. This angular discretization is validated by a parametric study in laboratory scale tests dedicated to radiative heat transfer [26].

The water spray model is calibrated on the basis of droplet size measurements performed with PDA technique [27]. In few words, this technique is based on light scattering interferometry and the Droppler effect. Measurements are made in a limited volume where two focused laser beams intersect [8]. To calibrate the Lagrangian particles submodels, PDA analysis has been simulated with FDS code, by varying the mean diameter at the injection point. The simulated configuration is one spray injected in a closed room by a nozzle located at a central position of the room. FDS predictions and experimental measurements are then compared at five positions along the central axis, from 4 cm to 50 cm from the injection point (see Figure 5). At each location, comparison deals with Sauter diameter (by definition the ratio of the volume of a sample of droplets to the surface area of the same sample).

As shown on Figure 5, the best agreement appears to be obtained with the spray defined at the injection point with a hybrid law defined by a mean diameter and a Rosin–Rammler dispersion parameter equal to 40 μm and 2.85 respectively. Note that as measurements concern only the central spray, it is assumed in the

present study that sprays produced by the lateral orifices are similar to the central one.

In addition to water spray modeling, the main input data for the numerical simulation are the HRR curve, the global combustion reaction and the extraction volumetric flow rate. As in Ref. [22], the HRR curve is set (see Figure 4). Before mist activation, the interpolated function is calibrated from experimental heptane pool weight loss and oxygen consumption monitoring. After mist activation, HRR is deduced only from experimental oxygen consumption. The effect of water mist application on the heptane burning rate is represented by the experimental HRR curve. For this reason, FDS fire suppression model is not activated. Parameters defining the heptane combustion reaction (such as soot and carbon monoxide yields) are extracted from the reference [31]. The extracted gas volume flux at the downstream side is set to get a longitudinal velocity without fire of around 2.9 m/s, the incoming fresh air through the upstream opening being at ambient temperature.

3.3. Comparison Between Measurements and Predicted Values

This stage consists of estimating the FDS prediction of the tunnel fire environment when the mist system is activated, by evaluating the discrepancy between predicted and measured quantities. Comparison between predictions and measurements is based upon gas temperature and heat flux. The following figures show local gas temperature and local heat flux on the vertical centerline at several distances from the fire as predicted by the simulation and as measured in the fire test.

3.3.1. Before Mist Activation. The longitudinal velocity induces a sub-critical ventilation regime. Before mist activation, no smoke counterflow is expected and all the smoke would be pushed away to the downstream side inducing a thermally stratified environment (see Figure 6). However, whereas ventilation velocity is higher at the initial time than the expected backlayering value, a short smoke counterflow is observed during the experiment after 100 s. As illustrated by the upper left subfigure on Figure 6, its thickness does not exceed 40 cm, 3 m upstream of the fire, and its length is comprised between 5 m and 9 m.

The CFD code does not predict this short backlayering upstream of the fire location. Downstream, comparison of predicted temperatures with measurements shows satisfactory general agreement for most of the locations: the slope and the magnitudes are similar (see Figure 6). The mean discrepancies over the time period [0;300 s] and over each section located downstream of the fire range between 25% and 31%. The comparison between predicted and measured temperatures confirms the previous observations reported in [26] for two other tests from the same campaign. First, agreement is better when the measurement section is away from the fire and temperature tends to be under-predicted in the flame region (see Figure 6). Secondly, bigger discrepancies are observed at mid-height in the mixing zone between the hot smoke layer in the upper part and the fresh air in the lower part. This area is better predicted by reducing the grid cell size but the corre-

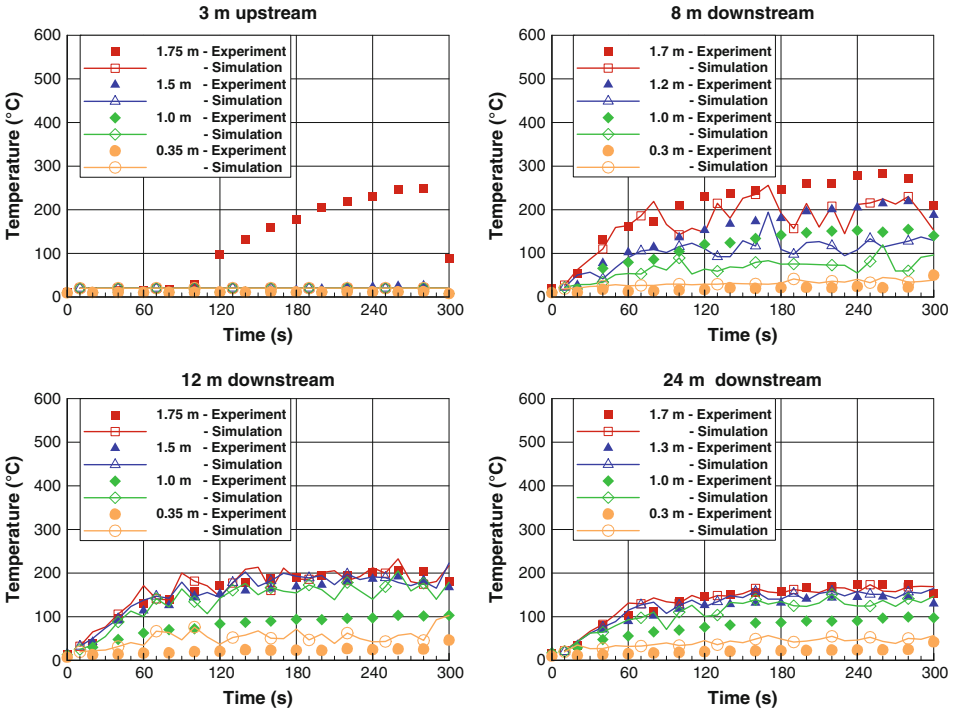

Figure 6. Before mist system activation, predicted and measured temperature versus time on the *vertical center line* of four measurement sections (*point* for experimental data and *solid line* for simulation).

sponding computational time is very long. The numerical data being considered as sufficiently close to measurements, the refined grid is not used in the present study.

Concerning radiative fluxes emitted by flames, gases and tunnel surfaces, they are measured on two measurement sections equidistant from the fire location (see Figure 7). The CFD code captures well the discrepancy in values measured upstream and downstream, induced by the longitudinal ventilation which tilts flame and plume. Moreover, it predicts well their temporal evolution: they are almost constant upstream while their evolution follows fire heat changes downstream. However, whereas the absolute difference between measurements and predictions is low upstream (below 0.17 kW/m^2), heat fluxes are slightly overpredicted by the code downstream of the fire.

3.4. After Mist Activation

Mist system activation induces the disappearance of counter-flow upstream of the fire (see Figure 8). Downstream of the fire location, the gaseous phase is cooled. Thus, temperatures decrease and become more uniform over the measurement

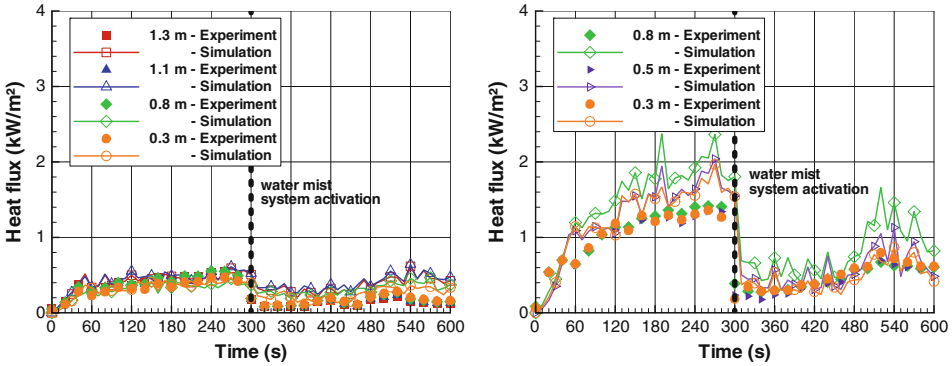

(a) 7 m upstream **(b)** 7 m downstream

Figure 7. Radiative fluxes versus time on the *vertical center line* of two measurement sections (*point* for experimental data and *solid line* for simulation).

section. For instance, temperatures are around 60°C at 8 m from the fire between 360 s and 400 s. This homogeneity in the gas temperature over each measurement section highlights a thermal destratification. Then, 2 min after mist system activation, the environment tends to be stratified again when HRR increases. Gas temperatures are indeed higher in the upper part than in the lower part. For instance, at 8 m from the fire and at 540 s, temperature is around 160°C close to the roof, 120°C at mid-height and 80°C below a height of 30 cm.

At all locations, temperatures decrease and their evolution after mist activation is closely reproduced in the simulation, even between 340 s and 480 s when the gas temperature is almost constant while HRR changes or after, when temperatures increase with HRR around 540 s. Concerning heat fluxes, their decrease at mist activation and their following evolution are well captured : the mean discrepancy over (300 s; 600 s) at all measurement points is lower than 0.25 kW/m^2.

4. Interaction of Water Mist, Tunnel Longitudinal Ventilation and Hot Smoke Flow

Once the test simulation is achieved, the computational tool is used intensively in order to improve the understanding of the interaction phenomena between water mist, tunnel longitudinal ventilation and hot smoke flow. In other words, the impact of water spray on tunnel air flow and thermal environment is looked into details. Vice versa, the impact of the ventilated tunnel fire environment on (liquid and vapor) water transportation and its evaporation is studied.

4.1. Effect of Water Spray on Tunnel Air Flow

Figure 9 presents the temporal evolution of gas flow rates at several distances from the fire. Before mist activation, at a given time, the gas mass flow rate is

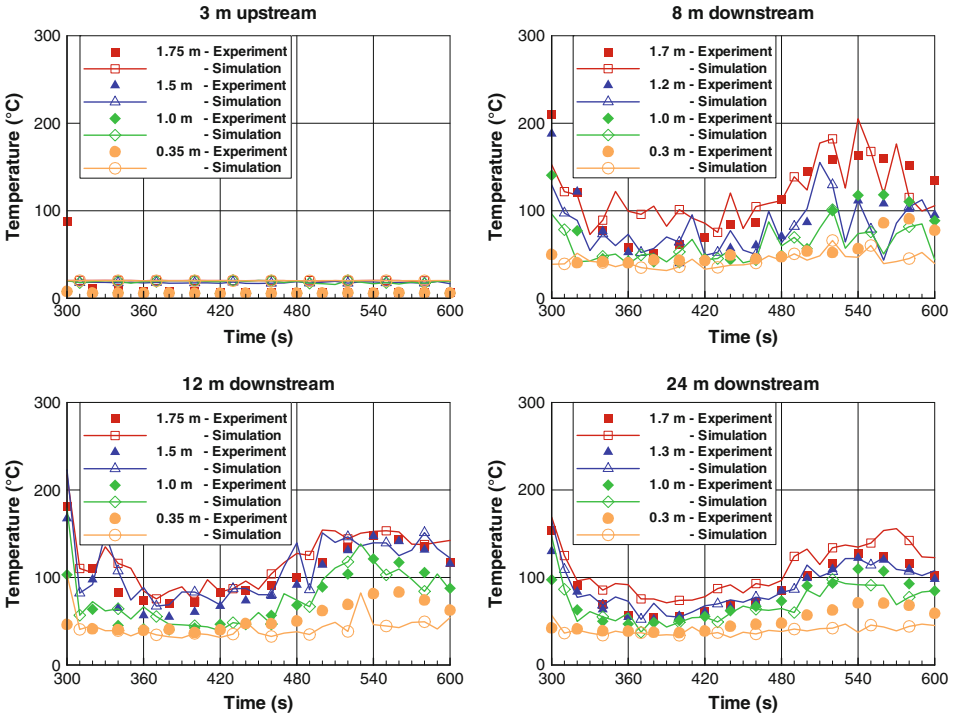

Figure 8. After mist system activation, predicted and measured temperature versus time on the *vertical center line* of four measurement sections (*point* for experimental data and *solid line* for simulation).

constant along the longitudinal direction. Mass conservation is also verified (the mass created at the fire location is relatively low). Concerning the volumetric gas flow rate, the one predicted downstream is not uniform along the longitudinal direction due to heat transfer to tunnel walls. The farther from the fire the measurement section is, the lower the gas flow rate is. Moreover, Figure 9 shows the large difference in volumetric rates between the upstream and the downstream tunnel parts. Rate is very low upstream in comparison with the downstream values. Moreover, the rate has the inverse evolution of HRR (decrease followed by a level-off) upstream whereas it is almost constant downstream. These two differences are attributed to the way of setting a longitudinal air flow (a constant volumetric gas volume flux is extracted at the downstream extremity), gas displacement also varies upstream with HRR. The large difference in values is promoted by the supercritical ventilation regime, the gas density being really higher upstream than downstream.

Mist activation induces a large increase in mass and volumetric flow rates upstream of the fire due to the strong gas cooling in the downstream part. A large mass of gas is thus transported from the upstream side to satisfy the boundary condition at the downstream extremity. Then, mass and volumetric flow rates

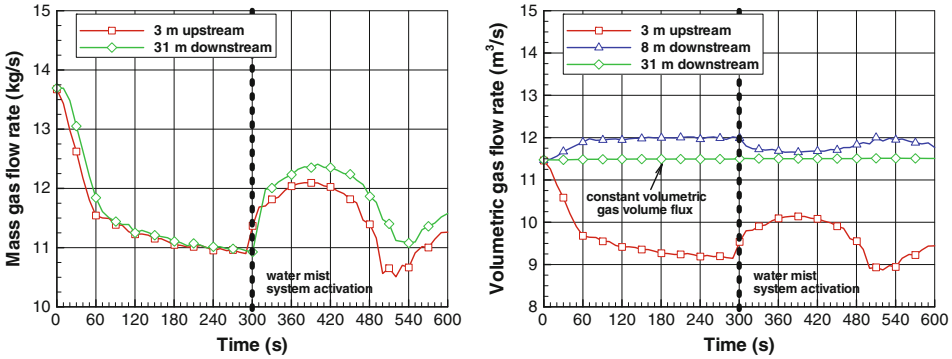

Figure 9. Gas flow rates versus time in mass (*left*) and in volume (*right*) simulated at several distances from the fire.

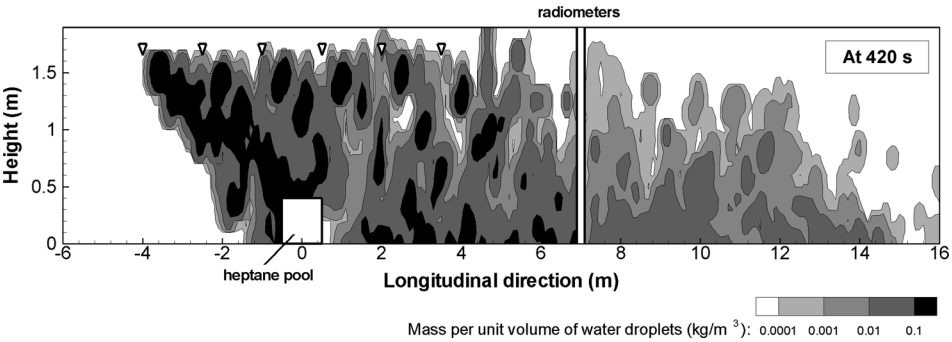

Figure 10. Contours of liquid water concentration on mid-plane in the tunnel at 420 s. *Triangles* indicate nozzle positions.

simulated upstream follow the inverse evolution of HRR whereas the volumetric flow rate is almost constant downstream. Note that after mist activation, the gas mass flow rate is not uniform anymore along the longitudinal direction, due to water mist evaporation.

4.2. Effect of Ventilated Tunnel Fire Environment on Water Transportation

Figure 10 presents contours of liquid water concentration on mid-plane 420 s after ignition i.e. 120 s after mist activation. This figure illustrates the transportation of the water droplets. Whereas the activated nozzles operate from 4 m upstream to 3.5 m downstream of the fire location, water droplets are transported up to 16 m downstream. The two-phase flow containing water vapor and smoke also acts as a radiative shield. It explains the low heat fluxes measured and predicted downstream of the fire during mist application while HRR is high (see Figures 4, 7).

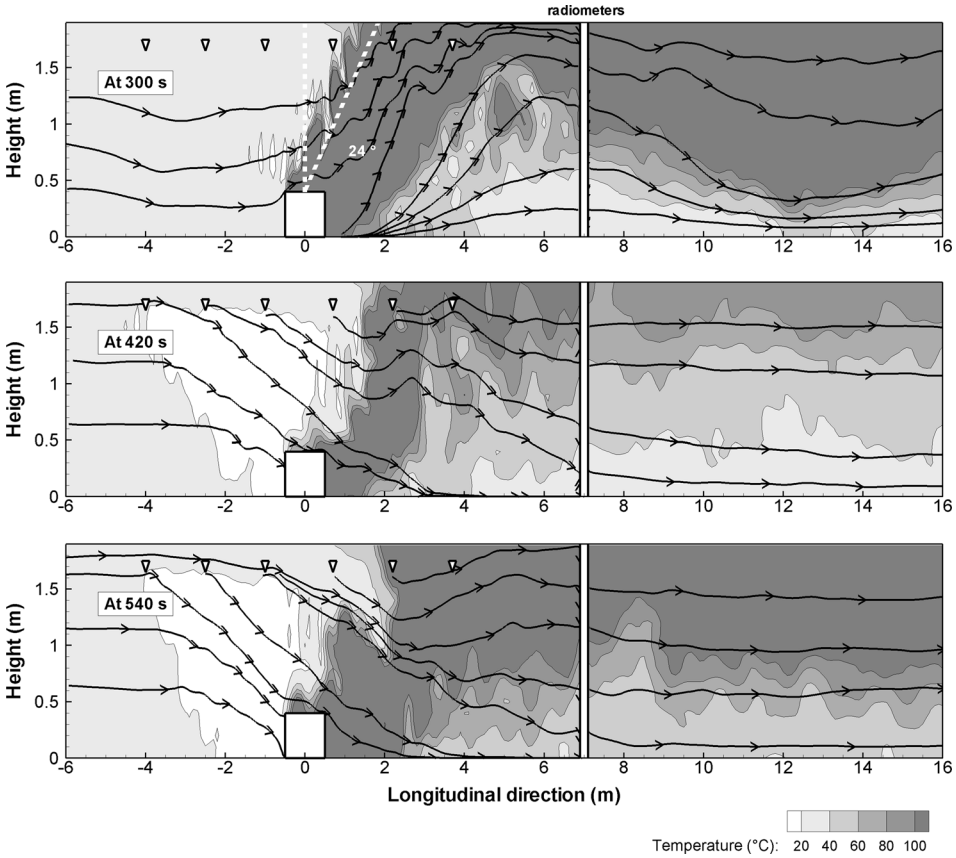

Figure 11. Contours of gas temperature on mid-plane in the tunnel at mist activation, at 2 min and at 4 min after mist activation.

4.3. Effect of Water Spray on Thermal Environment

Sprays lead to significantly different longitudinal flow and behavior of the fire plume. Indeed, fire plume is inclined and elongated in the longitudinal direction toward the downstream extremity at mist activation. After mist activation, sprays act as a shield to gas flow due to longitudinal ventilation and fire activity (see streamlines on Figure 11). The fire plume is also pushed down and strongly cooled down. Gas temperatures close to the fire are consequently very low in comparison with HRR value. For instance, when HRR is around 1300 kW at 420 s, the simulated temperature is comprised between 30°C and 135°C at 4 m from the fire and between 30°C and 90°C at 8 m.

Figures 11 and 12 with temperature contours confirm what is supposed above on the basis of local temperatures. Firstly, mist activation alters thermal stratification significantly, and the vertical temperature gradient is also very low. Secondly, by the end of the simulation, when HRR is high despite the water injection, the

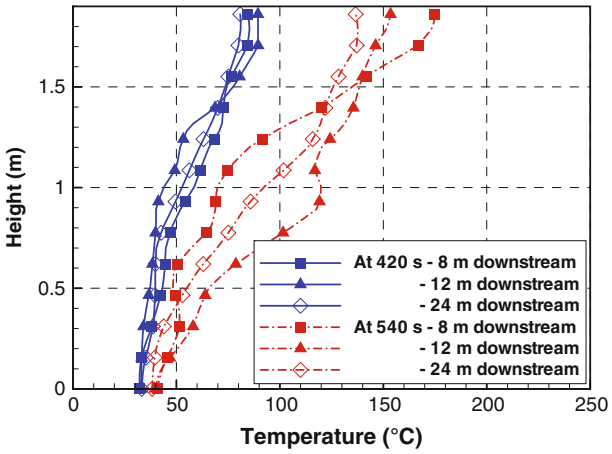

Figure 12. Profiles of air temperature along the *vertical center line* of three measurement sections 2 min and 4 min after mist activation.

environment tends to be thermally stratified and there is an obvious thermal gradient along the vertical axis. The closer the measurement section from the fire is, the clearer the vertical gradient is. It means that the hot gas in the upper part tends to get colder (upon contact with tunnel walls and due to the mist thermal contribution) and to mix with the fresher air in the lower part as it is flowing in the downstream direction.

5. Quantification of the Phenomena Involved

Section 3 demonstrates a good capability of the FDS code to simulate the test. Local measurements of gas temperature and heat fluxes highlight the heat contribution of water mist too. Thus, the following section aims at quantifying this contribution and understanding how this heat is absorbed. In a more general way, this section studies the energy distribution in the whole tunnel.

5.1. Theory

Global energy balance can be computed for the whole tunnel by extracting and collecting information from FDS calculation. The conservation of energy, drawn on Figure 13, holds that the fire heat release Q_{fire}:

- heats the gases within the control volume, noted Q_{gas},
- is transferred to boundaries by radiation and convection, noted Q_w,
- is transported through the openings, noted Q_d,
- is absorbed by the droplets, noted Q_{pg}.

The contribution to the gas heating is expressed as the time derivative of the gas enthalpy integrated over the whole domain

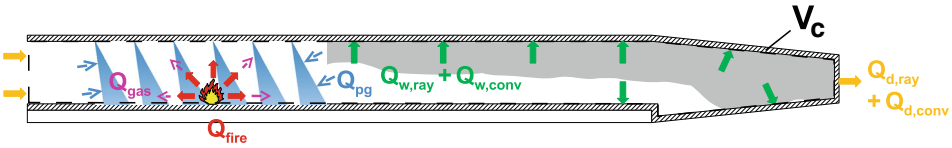

Figure 13. Global energy balance principle in the intermediate tunnel (Q_{fire} for fire heat, Q_{gas} for heat accumulated by heating gas, Q_w for heat loss to surfaces, Q_d for heat transported through the openings and Q_p for heat absorbed by droplets).

$$Q_g = \frac{\partial}{\partial t} \int_{\text{domain}} \rho C_p T_g \mathrm{dV} \tag{1}$$

where dV is the elementary volume of a control volume.

The wall heat exchanges by convection and radiation are evaluated as

$$Q_w = \int_{\text{wall}} h(T_g - T_w)\mathrm{dS} + Q_r \tag{2}$$

where h is a convective heat transfer coefficient evaluated by the default code from a combination of natural and forced convection correlations, dS is the elementary wall surface and Q_r is the radiative flux received by the wall (incoming flux minus outcoming flux computed with the default code), T_g is the gas temperature in the center of the first gas phase cell near the wall and T_w is the wall surface temperature.

Fluxes at the inlet and outlet are computed as

$$Q_d = \int_{\text{outlet}} \left(\rho \cdot u \cdot C_p \; T_{g,\text{outlet}} \mathrm{d}S\right) - \int_{\text{inlet}} \left(\rho \cdot u \cdot C_p \, T_0 \, \mathrm{d}S\right) \tag{3}$$

The last one Q_{pg}, can be expressed versus the energy absorbed over the phenomena described in introduction between gaseous and liquid phases

$$Q_{pg} = Q_{conv,p} + Q_{ray,p} \tag{4}$$

where $Q_{ray,p}$ is the radiative heat absorbed by the droplets. FDS approximates this term as follows:

$$Q_{pg} \approx h_{p,g} \cdot (T_p - T_g) S_p \tag{5}$$

where $h_{p,g}$ is the heat transfer coefficient between droplets at temperature T_p and the gaseous phase at temperature T_g [23].

Note that the total heat absorbed by the droplets for heating and vaporizing them, noted Q_p, is given by

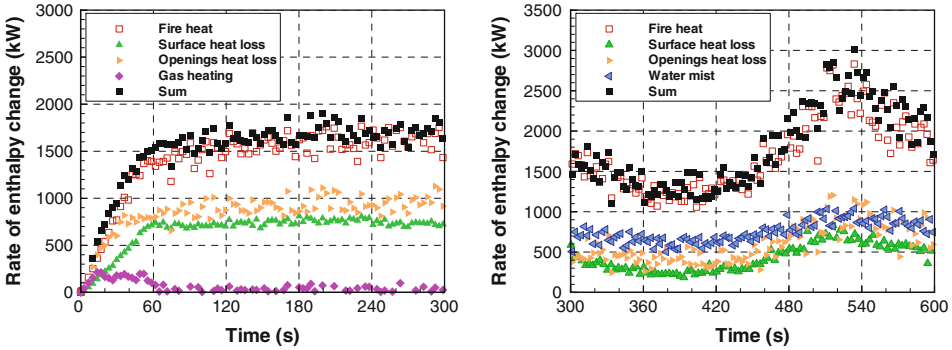

(a) Before water mist activation **(b)** After water mist activation

Figure 14. The rate of heat loss to surfaces (*filled triangle*), through the openings (*filled right pointing triangle*), accumulated by heating the gas (*filled diamond*), absorbed by droplets (*filled left pointing triangle*) and their sum (*filled square*) versus time. For comparison, the heat release rate is also shown (*open square*).

$$Q_p = Q_{p,g} + Q_{ray,p} + Q_{p,w} \tag{6}$$

where $Q_{p,w}$ gives the cooling energy of the solid surface due to droplets.

5.2. *Application to Numerical Results*

Figure 14a illustrates this energy distribution as a function of time before mist activation. For comparison, the heat release rate is also shown on this figure. Besides, energy can be considered as conserved in the control volume in both tests because the sum of wall loss, opening loss and energy is equal to fire heat. Figure 14a highlights that nearly the half quantity of fire heat is lost toward tunnel walls (46%) and the remaining heat is transported by the gases through the openings (52%). This heat distribution which is similar to the one in the test reported in Ref. [26] illustrates the confined situation of tunnel fires.

Figure 14b illustrates the energy distribution as a function of time after mist activation. Heat for heating/cooling gases in the control volume is not plotted since it is very low over this time duration in these tests: it represents −0.5% of fire heat thus showing a global gas cooling.

Local data seem to indicate in Sect. 3 that water mist plays a thermal role. Figure 14b confirms this observation which even appears important. Indeed, roughly the half quantity of fire heat is absorbed by droplets. The remaining quantity goes to heat tunnel surfaces (24%) or is conveyed by hot gases out of the tunnel (33%).

5.2.1. Heat Transfer to Surfaces. Figure 15 presents the temporal evolution of heat loss to solid surfaces by convection and radiation. Before mist activation, it

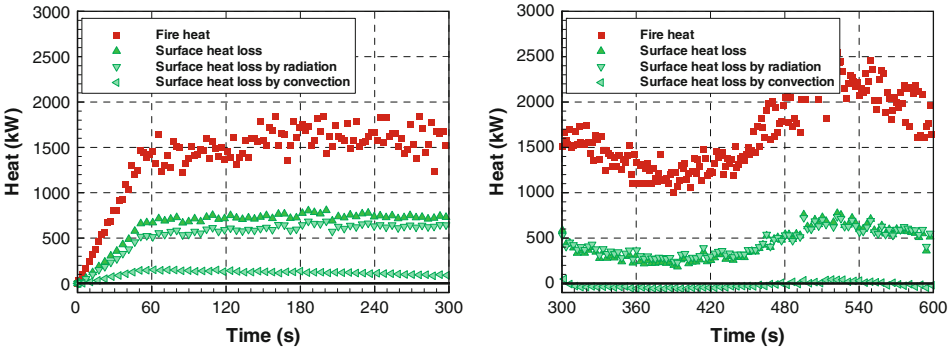

(a) Before mist activation **(b)** After mist activation

Figure 15. Rate of heat loss to surfaces by radiation and convection. For comparison, the global heat loss is also shown.

shows that heat transfer is mainly radiative: it represents 38% of HRR whereas the convective heat transfer to surfaces represents 8%. After mist activation, heat transfer to surfaces remains mainly radiative. However, Figure 15 shows that heat transfer to surfaces by convection is negative during mist application. Its mean value is equal to −1.4% over (300 s; 600 s) that is to say heat is mainly transferred from tunnel walls to gaseous phase.

In order to understand this particularity, the tunnel is divided into three zones in the longitudinal direction, the upstream and downstream parts being separated by the fire region. The fire region is defined as the zone where the released heat is higher than 0 kW. The rate of heat loss to surfaces in these three zones is plotted on Figure 16. Note that heat transfer in the upstream part is very low since the ventilation regime is supercritical. It appears that before mist activation, heat transfer by convection is mainly performed in the downstream zone where hot smoke is flowing along the tunnel roof toward the ventilation system. In the fire region, values are negative thus showing that tunnel walls are hotter than the gaseous phase since walls are still absorbing radiation emitted by the fire (see Figure 16b).

In the test studied, gas cooling due to water mist is important from the fire location up to the downstream extremity and in particular the fire plume is cooling greatly. Thus, heat transfer to walls drops in the downstream part, both by convection and radiation. At the fire location, despite the fire plume cooling, tunnel walls remain hot and in particular hotter than gas till 500 s. Consequently, heat is still transferred from tunnel walls to the gaseous phase in the fire location. However, in addition to gas cooling at the fire location, water droplets act as a radiative shield. Consequently, heat transferred to tunnel walls there by radiation decreases deeply and thus, tunnel walls are cooled down over the period (300 s to 500 s). Then, after 500 s, HRR increases greatly inducing hotter fire plume and smoke downstream of the fire (see Figure 8). Consequently, the convective heat increases in the fire region and in the downstream part until it becomes positive on the whole.

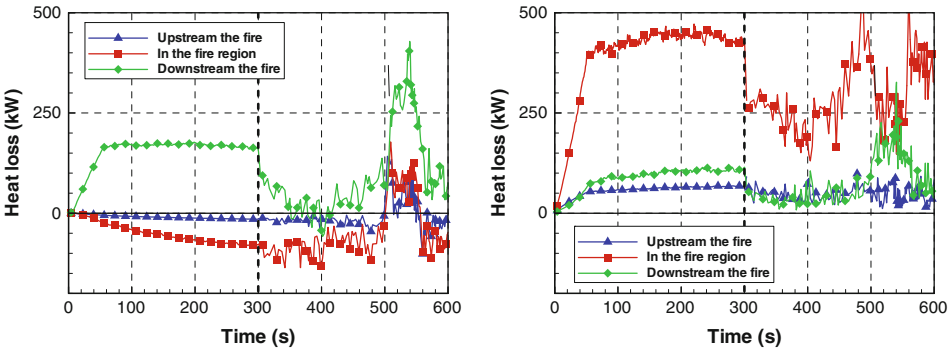

Figure 16. Rate of heat loss to surfaces predicted in the upstream zone, in the fire region and in the downstream zone.

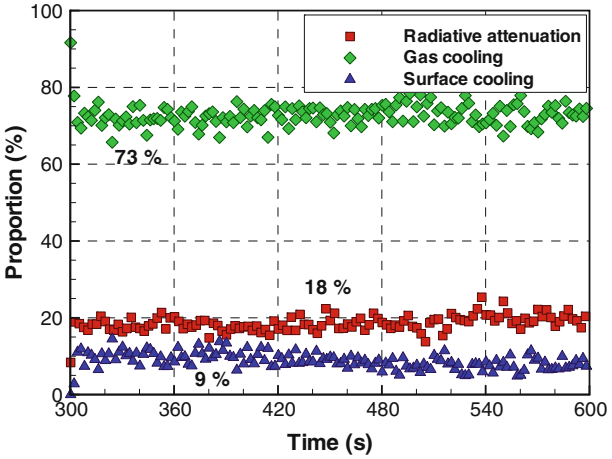

Figure 17. The rate of radiative attenuation (*filled square*), gas cooling (*filled diamond*), and surface cooling (*filled triangle*) versus time.

5.2.2. Heat Absorption by Water Mist. The use of the computational code has allowed us to quantify the heat contribution of water mist. It allows us to get a better understanding of how this heat is absorbed too. Three phenomena are also distinguished: radiative attenuation, gas and surface cooling. The ratio of heat absorbed by each phenomenon with the total heat absorbed by water Q_p is plotted on Figure 17. Also, the heat absorbed by droplets mainly comes from the gaseous phase (73%). More precisely, 73% of the energy absorbed by water droplets induces gas cooling. The last 27% of fire heat absorbed by droplets results from radiative attenuation (18%) and surface cooling (9%).

6. Conclusion

The present work is an example of use of a CFD code. based on the experimental conditions like HRR versus time, it focuses on improving the understanding of the interaction phenomena between water mist and fire in tunnels. For this purpose, the work makes an extensive use of the computational tool FDS developed by NIST (version 5.4). The approach consists of numerically reconstructing one fire test conducted in a model tunnel (1:3). The test was carried out with a supercritical longitudinal ventilation regime which avoids the occurrence of the backlayering phenomenon. Water mist was produced by six nozzles located on both sides of the fire location. The use of such a reduced scale allows in particular the setting up of a large number of sensors to characterize the fire environment.

The simulation of the fire tests allows us to assess the accuracy of the CFD tool in this configuration. The evaluation is based on a comparison of predicted and measured temperatures and heat flux at several distances from the fire location. Before the activation of the water mist system, the numerical simulation shows a satisfactory general agreement for gas temperatures at most locations: the slope and the magnitudes are similar. Moreover, the simulation confirms the spatial variation of the agreement already reported in [26]. After the activation of the water mist system, the CFD code predicts the large reduction of gas temperatures and heat fluxes at mist activation similar to that measured and their evolution afterwards.

Extraction and collection of information from FDS computation make it possible to study the interaction of water mist, tunnel longitudinal ventilation and hot smoke flow. The water mist system operation strongly affects the tunnel gas flow due to water vapor production and strong gas cooling. Then, droplets are predicted to be displaced by the air flow over more than 10 m in the downstream direction. This water mist in suspension in the gaseous phase acts as a radiative shield and explains the low measured heat fluxes. Last, CFD code predicts that the tunnel environment can remain thermally stratified despite mist application.

Furthermore, data post-processing allows us to understand the heat distribution within the tunnel. Without water mist, it illustrates the confined situation of tunnel fires. With water mist, it highlights the strong thermal role played by mist which represents half of the fire heat. In addition, this data post-processing allows us to assess the importance of certain mechanisms involved when water is sprayed in a tunnel fire environment, namely gas and surface cooling or radiative attenuation. It also shows the importance of gas cooling which represents in the test studied 73% of the total heat absorbed by water droplets. In practice, it means that a numerical developer must pay attention to modeling this phenomenon.

Finally, the present work raised many questions and remarks. For instance, the computational study should be extended to more detailed computation in order to assess the choice of the CFD model and the importance of the tunnel scale ratio on the quantitative results of the present study. Moreover, in the next campaigns, other measurements should be investigated in order to appreciate water droplet displacement (by covering the floor with small pans), the energy distribution (by installing thermocouples within the walls), and the amount of evaporated water quantity (by measuring gas humidity downstream of the fire).

Acknowledgment

First of all, the authors would like to thank the French agency ANRT for the funding of E. Blanchard during her PhD work. They also want to thank E. Cesmat, R. Meyrand and the French authorities DDSC and CETU for having investigated and greatly contributed to the research project.

References

1. Working Group 6 Ventilation and Fire Control of the Technical Committee C3.3 Road Tunnel Operations (2008) Road tunnels: an assessment of fixed fire fighting systems. Technical report 2008R07, World Road Association PIARC , La défense
2. NFPA 750 (2010) Standard on water mist fire protection systems
3. Grant G, Brenton J, Drysdale D (2000) Fire suppression by water sprays. Prog Energy Combust Sci 26(2):79–130
4. Collin A, Boulet P, Parent G, Lacroix D (2007) Numerical simulation of a water spray—radiation attenuation related to spray dynamics. Int J Therm Sci 46:856–868
5. Modest MF (1978) Radiative heat transfer, 2nd edn. Mc Graw-Hill International Editions, New York
6. Garo JP, Vantelon JP, Lemonnier D (2010) Effect on radiant heat transfer at the surface of a pool fire interacting with a water mist. J Heat Transf 132(2):79–130
7. Lönnermark A (2005) On the characteristics of fires in tunnels. PhD thesis, Lund University, Lund
8. Husted PB (2007) Experimental measurements of water mist systems and implications for modelling in CFD. PhD thesis, Lund University, Lund
9. Kincaid DC, Longley TS (1989) A water droplet evaporation and temperature model. Trans Am Soc Agric Eng (ASAE) 32(2):457–463
10. Lechêne S, Acem Z, Parent G, Jeandel G, Boulet P (2011) Upward vs. downward injection of droplets for the optimization of a radiative shield. Int J Heat Mass Transf 54:1689–1697
11. Liu Z, Carpenter D, Kim AK (2006) Characteristics of large cooking oil pool fires and their extinguishment by water mist. J Loss Prev Process Ind 19:516–526
12. Back GG, Beyler CL, Hansen R (2000) A quasi-steady-state model for predicting fire suppression in spaces protected by water mist systems. Fire Saf J 35:327–362
13. Kratzmeir S, Starke H (2007) Safety of life in tunnel—final report. Technical report, UPTUN
14. Opstad K (2004) Evaluation of current mitigation technologies in existing tunnel—final report. Technical report, UPTUN
15. Mawhinney JR (2011) Fixed fire protection systems in tunnels: issues and directions. Fire Technol 47:1–32
16. Heskestad G (2002) Scaling the interaction of water sprays and flames. Fire Saf J 37:535–548
17. Quintiere JG, Su GY, Schultz N (2007) Physical scaling for water mist fire suppression—a design application. Int J Eng Perform Based Fire Codes 9(2):87–108
18. Ingason H (2008) Model scale tunnel tests with water spray. Fire Saf J 43(7):512–528
19. Chen L, Zhu W, Cai X, Pan L, Liao G (2009) Experimental study of water mist fire suppression in tunnels under longitudinal ventilation. Build Environ 44:446–455

20. Hart RA (2005) Numerical modelling of tunnel fires and water mist suppression. PhD thesis, Nottingham University, Nottingham
21. Nmira F (2007) ModTlisation et simulation numTrique de l'interaction entre un feu et un brouillard d'eau. PhD thesis, UniversitT de Provence, Marseille
22. Trelles J, Mawhinney JR (2010) CFD investigation of large scale pallet stack fires in tunnels protected by water mist systems. J Fire Prot Eng 20:149–198
23. McGrattan KB, Hostikka S, Floyd JE, Baum H, Rehm R, Mell WE, McDermott R (2011) Fire dynamics simulator, technical reference guide, volume 1: mathematical model. NIST special publication 1018-5, National Institute of Standards and Technology, Gaithersburg
24. McGrattan KB, McDermott R, Hostikka S, Floyd JE (2010) Fire dynamics simulator, user's guide. NIST special publication 1019-5, National Institute of Standards and Technology, Gaithersburg
25. Meyrand R (2009) Étude sur l'usage de brouillards d'eau en milieu tunnel—Travail en réduction d'échelle. PhD thesis, École Nationale Supérieure de Mécanique et d'Aérotechnique, Poitiers
26. Blanchard E, Boulet P, Desanghere S, Cesmat E, Meyrand R, Garo JP, Vantelon JP (2012) Experimental and numerical study of fire in a midscale test tunnel. Fire Saf J 47:18–31
27. Ponticq X (2008) Études sur les systFmes fixes d'aspersion d'eau en tunnel. PhD thesis, UniversitT Claude Bernard, Lyon
28. Babrauskas V, Grayson SJ, Janssens M, Parker WJ (1992) Heat release in fires. Elsevier, Amsterdam
29. McGrattan KB, Hamins A (2001) Numerical simulation of the Howard Street tunnel fire (Baltimore, Maryland). Technical report 6902, National Institute of Standards and Technology, Gaithersburg
30. Cochard S (2003) Validation of fire dynamics simulator (version 2.0) freeware. Tunn Manag Int J 6(4)
31. Tewarson A (2002) SFPE handbook of fire protection engineering, 3rd edn. National Fire Protection Association, Quincy